



A Study on Forced-Air Thermal Dissipation in Lithium-Ion Batteries Using Numerical Method

Khai H. Nguyen, Tung X. Vu, Le Thi Thai, and Van-Sang Pham^(✉)

School of Transportation Engineering, Hanoi University of Science and Technology,
No 1. Daicoviet Road, Hai Ba Trung Dist, Hanoi 100000, Vietnam
sang.phamvan@hust.edu.vn

Abstract. The battery temperature management system is crucial to battery performance, affecting the entire functionality of the electric vehicle's powertrain system (EVs). Air-cooling is extensively utilized in EVs due to its advantages in structure design, high reliability, and safety. In this work, we investigate the heat dissipation of a battery module using the forced-air method. The simulation results showed that the best thermal dissipation operational state for the battery system is at a lower vehicle speed of 36 km/h. Also, since the battery generates more heat at 72 km/h, the optimal working condition in this regime is SOC greater than 36%.

Keywords: Battery · Thermal dissipation · Forced-air

1 Introduction

Climate change has caused problems for the transportation industry in recent years. Traditional vehicles do not just consume a lot of petroleum, but they already release a lot of solid suspended particles, hydrocarbons, nitrogen oxides, and sulfur oxides, all of which are major pollutants in the environment. New energy vehicle development can efficiently address issues such as fossil fuel shortages, automotive emissions, and environmental damage [1–6]. Since the environmental benefits, high efficiency, safety, and long-term endurance, electric automobiles, nowadays, are receiving increasing attention [7–10]. However, despite the benefits, BEVs confront major obstacles. When temperatures rise over an acceptable level, Lithium-Ion Batteries (LIBs) degrade quickly, increasing the risk of fire and explosion. During charging and discharging, lithium-ion batteries generate heat both inside the cells and in the interconnection points, resulting in excessive battery temperature rise and temperature non-uniformity.

In order to remove the excessive heat in the battery, much research has been conducted to develop an efficient BTMS for EVs and HEVs. Wang et al. [11] discussed the design considerations for BTMSs and described four types of BTMS cooling methods: air cooling, liquid cooling, PCM, and heat pipe cooling. Liquid cooling was suggested as being the most suitable method for large-scale battery applications at high charging/discharging C-rate and in high-temperature environments. A similar review was

conducted by Xia et al. [12]. Kim et al. [13] reviewed heat generation phenomena and critical thermal issues of lithium-ion batteries. The different BTMS cooling methods were proposed and categorized. Except for the air and liquid cooling techniques, the paper also presented refrigerant two-phase cooling, PCM-based cooling, and thermo-electric element cooling. It reported that the heat pipe system needs extra cooling plates with additional weight and volume to enlarge the contact areas with the battery cells. Liu et al. [14] summarized the development of BTMS systems including air, liquid, boiling, heat pipe, and PCM-based cooling with a particular focus on the PCM cooling techniques. Thanks to that, it was suggested that the improvement of BTMS systems should be focused on the performance and safety enhancement of Li-ion batteries.

Despite the preceding research looking at various cooling ways for batteries used in EVs and other applications, there is still a gap in the literature about air-cooled BTMSs for EVs and HEVs. The air-cooling BTMS is one of the most essential cooling options for making EVs and HEVs more efficient and safer. Its low cost and simple construction make it appealing for a variety of commercial EV and HEV BTMS applications. For all of these things, in this work, we will examine the effect of forced-air cooling on the battery package, which will provide information on a battery system’s pros and cons in usage.

2 Battery Package Modeling

2.1 Battery Model Construction

In order to examine the thermal states of the EV battery, we need to evaluate a specific battery model. In this paper, we refer to the Tesla Roadster Model S because it is not only a pioneer in EV vehicles but also the availability of Tesla patents in the public domain, which was useful in gaining a good grasp of battery module structure as well as its thermal mechanism.

A Tesla Model S battery pack is made up of 18650 (65 mm × 18 mm) individual Lithium-Ion cylinder cells, coupled in both series and parallel. This battery pack consists of 16 identical battery modules arranged in a 74p6s pattern. The 74p denotes a set of 74 cells that are connected in parallel and 6 s implies that six of these ‘74p groups’ are linked in a sequence [Fig. 1]. Thus, it generated an energy capacity of 5.3 kWh per module.

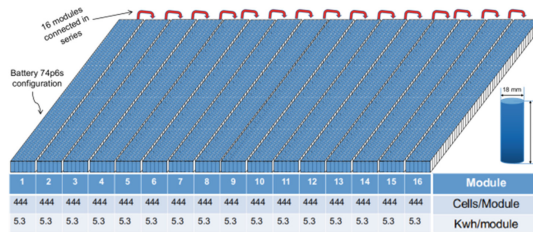


Fig. 1. A sketch of the tesla model S battery package

A battery module contains the cooling system, module management system, wiring, and other components are integrated within the battery module [20]. In the Tesla Model S, each module is made up of 444 cells coupling in a staggered grid to guarantee the working of the thermal management system. As a suggestion, this paper estimates the thermal dissipation of such an arrangement. However, due to the cell arrangement periodic property of the module as well to reduce the number of complexity in mathematics equations, we just analyze a group of 3 cells coupling in series, put in staggered grid [Fig. 2]. The parameters that affect temperature distribution such as the cell’s distance, the feed-flow rate, state of charge, will also be calculated.

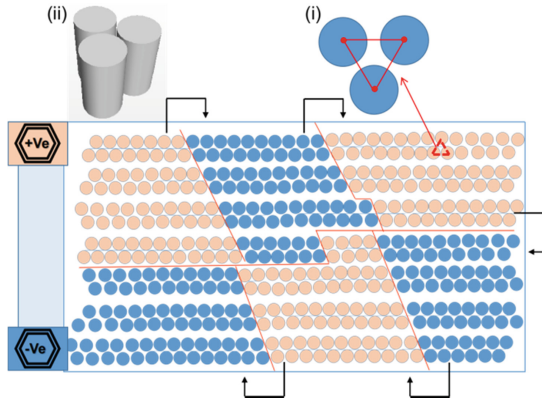


Fig. 2. The battery module arrangement in Tesla Model S. The cells are grouped up 6 segment coupling in series (the black arrow indicates series connector, the cells orange and blue color depict positive and negative side, respectively). Each series includes 74 cells connected in parallel. (i) - The typical group of cell arrangements in a module. (ii) - The estimating model.

2.2 Mathematical Model

2.2.1 Cell Heat Generation Modeling

During battery operation, the Newman-Tiedemann -Gu mathematical model [15–17] is utilized to describe the behaviors of the battery. Herein, the cell voltage follows Eq. 1, discharge progress described by Eq. 2, charge progress governs by Eq. 3 and Eq. 4. The total cycle of charge-discharge generates the amount of heat obeys Eq. 5.

$$V_{cell} = V(soc_i, T) - \frac{i}{\gamma(soc_i, T)} \tag{1}$$

$$SOC_i = 1 - (1 - SOC) \frac{C_{Ah.m^{-2}, 0}}{C_{Ah.m^{-2}, i}} \tag{2}$$

$$SOC_i = SOC \frac{C_{Ah.m^{-2}, 0}}{C_{Ah.m^{-2}, i}} \tag{3}$$

$$SOC = \frac{\int i dt}{C_{Ah.m^{-2}, 0}}; i = \frac{I}{A} \quad (4)$$

$$Q = I \cdot \left(U_{oc} - V_{cell} - T \frac{dU}{dT} \right) \quad (5)$$

where A is the electrode area (m^2). $C_{Ah.m^{-2}, 0}$ is nominal cell capacity ($Ah.m^{-2}$). $C_{Ah.m^{-2}, i}$ is cell capacity at current density i ($Ah.m^{-2}$). i - is current density ($A.m^{-2}$). I -is current (Amps). SOC is the state of charge (fraction). T is the temperature (K or $^{\circ}C$). U_{oc} is equilibrium voltage (V) and γ is admittance term ($Ohm^{-1}.m^{-2}$).

2.2.2 Battery Thermal Dissipation Modeling

Regarding the transport equation indicating the three-dimensional flow and heat transfer for Newtonian fluids, it is governed by Eq. 6, treated by integrating over a control volume V , and Gauss divergence theorem follows Eq. 7.

$$\frac{\partial(\rho\phi)}{\partial t} + div(\rho\phi U) = div(\Gamma grad\phi) + S_{\phi} \quad (6)$$

$$\frac{d}{dt} \int_A \rho\phi dV + \int_A \rho v\phi .da = \int_A \Gamma \nabla\phi .da + \int_V S_{\phi} .dV \quad (7)$$

where ϕ represents the scalar property being transported, including velocity components, pressure, energy. Γ is diffusion coefficient, described by Arrhenius-Eq. 8.

$$\Gamma = D_{eff} = D_0 e^{\frac{-E_a}{RT}} \quad (8)$$

Four terms in Eq. 7 show transient term, convective flux, diffusive flux, and the source term respectively. Herein, the transient term implies the rate of change of property ϕ in the control volume V . The convective flux indicates the total velocity of decrease of the fluid property across the volume boundary causing convection. Diffusive flux signifies the rise of the property within the control volume due to diffusion. And the source term depicts the generation/destruction of ϕ .

2.3 Numerical Solver and Mesh Resolution

In this work, the multi-solver is utilized to handle the interaction between cell heat generation and surface cell heating, as well as thermal convection from the heated cell surface and feed-flow. Four primary solver control models include *Implicit Unsteady*, *Reynolds-Averaged Navier-Stokes (RANS)*, *Battery*, and *Segregated Fluid Temperature*.

In the implicit method, nonlinear systems of algebraic equations are solved inter-actively for the value of all sub-volume at the new time simultaneously. Because high-frequency pressure fluctuations are not of concern in the cooling system, this approach is ideal for estimating. Also, due to the battery's discharge time, this simulation takes a long duration, so that large time steps must be set-up. The RANS turbulence model

gives a closure relationship for the Reynolds-Averaged Navier Stokes equations to solve for the transport of mean flow quantities. States of flow are obtained by decomposing the instantaneous quantities into a mean value and a fluctuating component (variable ϕ in Eq. 7). A battery solver is used to control the battery physics properties such as state of charge or heat generation. In the segregated fluid temperature model, the total energy equation is solved with temperature as the solution variable. The equation of state is then used to calculate enthalpy from temperature. Thus, the heat transfer problem between the battery surface and the air-feed flow is described using this model.

In this work, the estimating model is meshed automatically by a polyhedral mesher, the base's size 5 mm. Total time takes 171 s, acquired 1849.99 MB. The number of cells are 126087, faces are 666509, and vertices are 620067 [Fig. 3]. All cases are conducted on Desktop Dell VOSTRO 64-bit, 8 GB Ram, processor Intel Core i3-4170 CPU @ 3.70 Ghz.

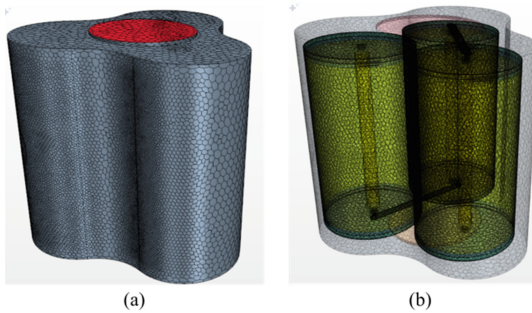


Fig. 3. Battery model meshing. (a) Casing mesh and (b) Cells mesh.

2.4 Boundary Conditions

In this model, to examine the effect of forced airflow on the battery dissipation performance, we shall determine multiple cases. Where the boundary condition is applied includes velocity = 20 m/s at case inlet, zero gradient pressure at case outlet. Battery region for the cells, Ohmic heating for the connector, and strap. And wall boundary conditions remain for the case pod.

3 Results and Discussion

In this work, we model three cells that correspond to a nominal battery module. Along with that, our estimation method uses three different vehicle speeds to identify the thermal states. The three vehicle-operation regimes are 10 m/s (36 km/h), 20 m/s (72 km/h), and 30 m/s (108 km/h).

During the defining battery process, a parameter known as C-rate is typically used to quantify the rate at which a battery charges or discharges. The C-rate (units of h^{-1}) is computed by dividing the current (A) by the nominal capacity (Ah) following:

$$C - rate = \frac{Current(A)}{Capacity(Ah)} (h^{-1}) \quad (9)$$

The three equivalent C-rates of the model are derived as Fig. 4 refers to the Tesla Range Plotted Relative To Speed publication and the formula Eq. 9.

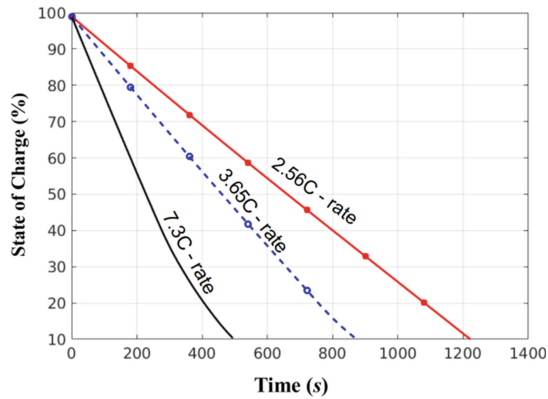


Fig. 4. Three of estimating battery discharge rates. In which 2.56C, 3.65C, and 7.3C respond to 495 (s), 990 (s) and 1406 (s), respectively.

It is noticed that the temperature nonuniformity of all of the cylindrical battery cells will have a serious impact on the battery's reliability, cycle life, electrochemical properties, and safety. According to the IEC 62133-2:2017 standard requirements, the allowable discharge battery temperature ranges from $-20\text{ }^{\circ}\text{C}$ to $60\text{ }^{\circ}\text{C}$. For lithium-ion battery temperatures, a temperature range of $25\text{ }^{\circ}\text{C}$ to $40\text{ }^{\circ}\text{C}$ was recommended, with a maximum temperature differential of about $5\text{ }^{\circ}\text{C}$ [18–22]. As a result, the paper will estimate the thermal properties of the battery in the following sections, utilizing this requirement as a reference to examine the battery's thermal dissipation capabilities.

3.1 Examination Thermal State of Model 2.56C Rate Discharge

The simulation of the battery at 2.56C ($I = 19.2\text{ A}$, $U = 20\text{ m/s}$) discharge rate is shown in Fig. 5. The surface temperature of cells in a group does not differ significantly, and the influence of varied cell spacing configurations has essentially little effect.

During the 20 m/s EVs constant speed, the battery surface temperature fluctuates in the range of $26\text{ }^{\circ}\text{C}$ to $35\text{ }^{\circ}\text{C}$, which is within the recommended temperature range for EVs [18–22]. Besides, as can be observed, the highest cell differential temperatures ranging from $1.05\text{ }^{\circ}\text{C}$ to $0.4\text{ }^{\circ}\text{C}$ representing 1 mm, 2 mm, and 4 mm cell spacing in each test instance [Figs. 6], the effect of cell spacing in three circumstance-examinations is not significant. This is trivial when the vehicle's thermal behavior is taken into account. As a result, the forced-air approach method is ideal for EV cooling design in this regime.

Despite the low specific heat capacity of air cooling ($1.0035\text{ J}\cdot\text{g}^{-1}\cdot\text{K}^{-1}$), the advantages of the forced-air approach in EV thermal management in this regime offered significant benefits. Supplementarily, there is an interesting circumstance here in which increasing the cell distance appears to make the system hotter [Fig. 6a]. This can be explained by the pressure difference and velocity field, which are displayed in Fig. 7.

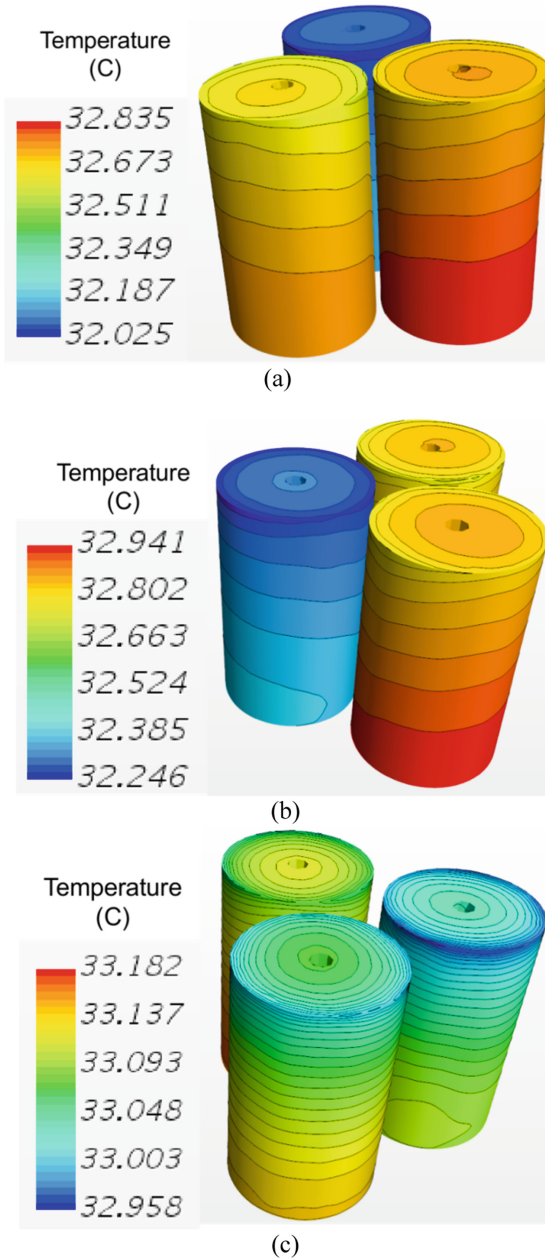


Fig. 5. Surface temperatures of 2.56C discharge rate at full discharge state (SOC = 0%). (a) A 1 mm cell spacing, (b) A 2 mm cell spacing, and (c) A 4 mm cell spacing.

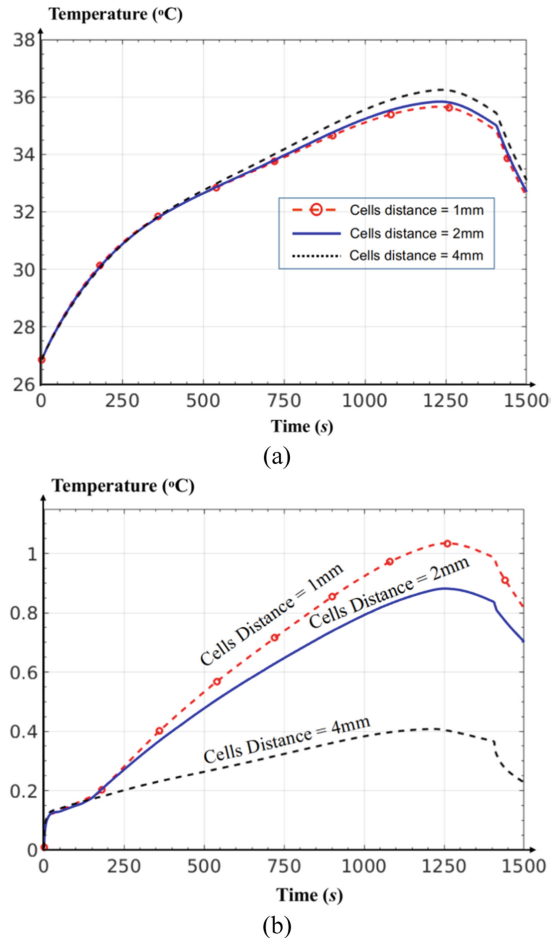


Fig. 6. The plot of 2.56 C discharge rate. (a) Surface average temperature and (b) differential temperature between cells in a circumstance.

Following that, the gradient pressure in the cases between inlet and outlet boundaries are approximately 3000 (Pa), 2200 (Pa), and 1700 (Pa) corresponding to 1 mm, 2 mm, and 4 mm, respectively [Fig. 7b, d, f]. Which causes the different velocity values inside the case. Specifically, the pressure is larger, the velocity is higher [Fig. 7a, c, e]. As a result, with the same contacting surface, the heat transfer in the narrower cell spacing is larger because the faster velocity yields the higher coefficient of heat convection ($Q = \alpha \cdot F \cdot (t_{\text{surface}} - t_{\text{flow}})$ - Newton Heat Law). Therefore, the average temperature of cells distance by 1 mm will be the lowest.

Despite that, cell temperature homogeneity was positive as cell distance increased. To explain this phenomenon, the strap connector is considered. In the model, the strap connector is used to link cells in one examine-circumstance. This is a factor that impacts velocity distribution within the case in the forced-air system. When cell spacing narrows,

this strap acts as an obstacle to flow movement, resulting in non-uniform cell velocity. As a result, heat dissipation is non-uniform. When cell spacing is larger, on the other hand, airflow can encroach on all available space within the case, as well as the area region between cells, where the strap's influence is minimal. Consequently, the larger cell spacing will have the best temperature uniformity [Fig. 6b].

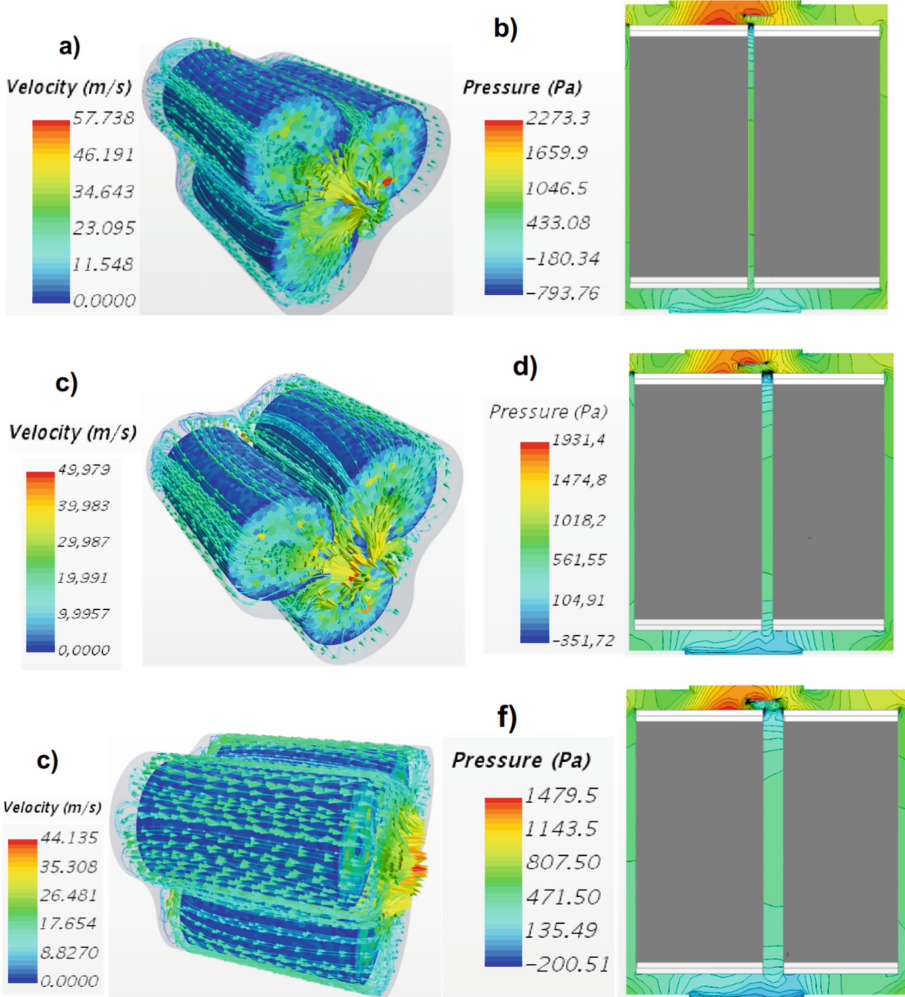


Fig. 7. The visualization of the battery velocity and pressure at 2.56C discharge rate for the 3-cell system mimics the actual operating in the vehicle. Where figures a, c, e indicate the velocity coolants of estimating-case, it is 1 mm, 2 mm, 4 mm cell-spacing respectively. The figures d, e, f show the pressure field at the corresponding arrangement, 1 mm, 2 mm, 4 mm serially.

3.2 Examination Thermal State of Model 3.65C Rate Discharge

Estimating the 3.65C discharge rate of the model, the battery temperature simulation results are presented in Fig. 8a, b, c. Comprehensively, following the increase of vehicle speed, the needed current rises, so that the battery heat generation goes up [Eq. 5]. Here, corresponding to 3.65C, the 27.4 A current value is extracted which ensures the vehicle speed at 30 m/s (72 km/h) constantly.

After computing the interaction between the surface battery and flow-air, as well as heat convection within the case, the acquired data indicated the increase in average battery temperature at three circumstances, roughly 28 °C and 44 °C [Fig. 9a]. This thermal range is higher in comparison to the prior operation mode. On the other hand, in this regime, the temperature differential between cells rose to 1.9 °C [Fig. 9b] for 1 mm cell spacing and 0.8 °C for 4 mm cell spacing.

For all of these factors, although it still guarantees the IEC 62133-2:2017 standard, the appropriate design to apply in the vehicle's heat dissipation at this speed should be carefully considered. It is the consistency of surface temperature and cell uniformity temperature, but also space-optimizing and safety.

As aforementioned, the influence of input flow rate, which is controlled directly by gradient pressure from the RANS method, causes the differential temperature inside the case. The velocity and pressure distribution within the case is depicted in Fig. 10. The narrower the space, the higher the velocity (or/also gradient pressure); therefore, the amount of heat dissipated rises.

In addition, according to the report data [Fig. 9a], the battery surface temperature can reach 44 °C, however, this is the highest temperature reached during the vehicle cycle life. Plot 9a shows that the battery temperature exceeds the safety point ($T = 40$ °C) after the 600th second (SOC = 35.8%). As a result, it is suggested that the battery SOC be kept at or above 36% during this regime to ensure the safety mode.

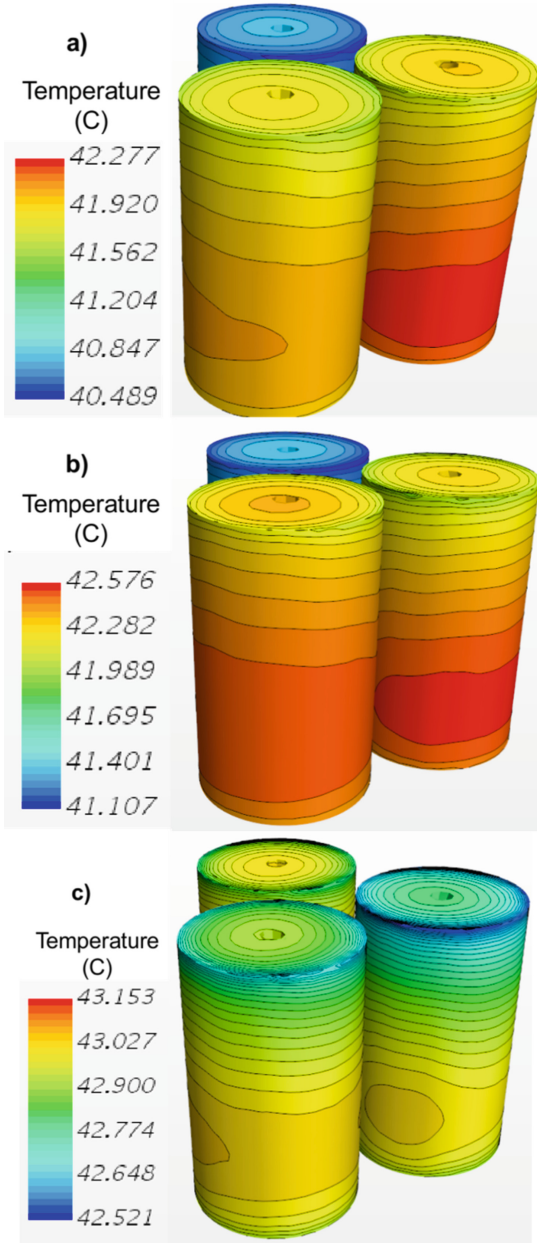
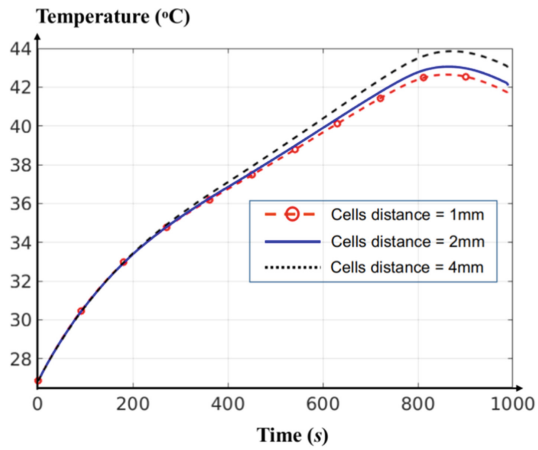
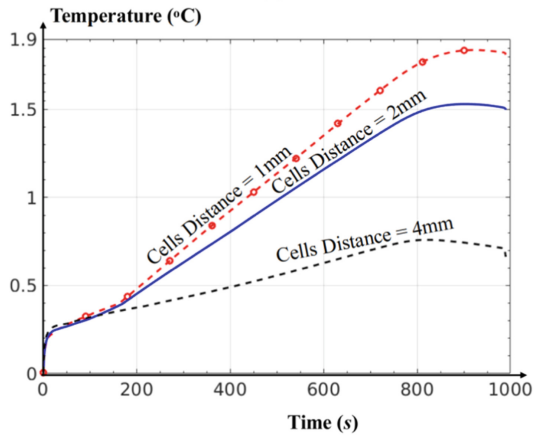


Fig. 8. The 3,65C visualization of battery temperature at full discharge state (SOC = 0%). (a) Cells spacing 1 mm, (b) cells spacing 2 mm, and (c) cells spacing 4 mm.



(a)



(b)

Fig. 9. The plot of 3.65C discharge rate for (a) average surface temperature and (b) differential temperature between cells in a model.

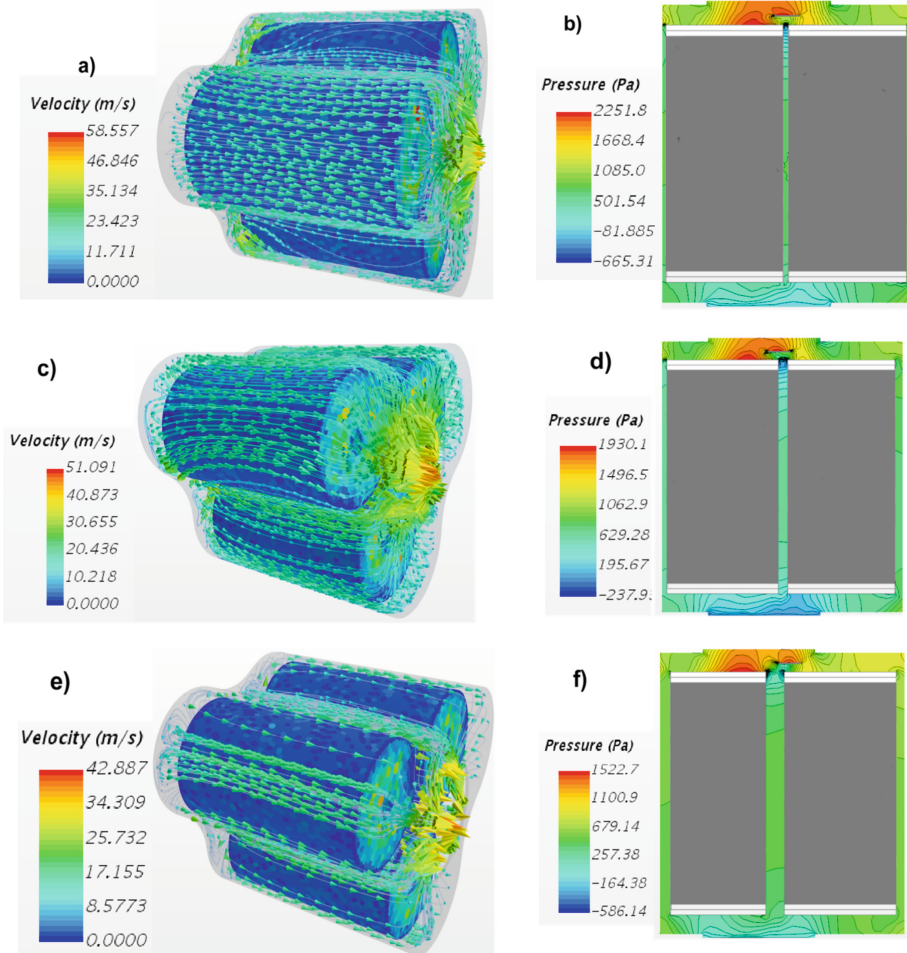


Fig. 10. The visualization of the battery velocity and pressure at a 3.65C discharge rate. Where figures a, c, e indicate the velocity coolants of estimating-case, it is 1 mm, 2 mm, 4 mm cell-spacing respectively. The figures d, e, f show the pressure field at the corresponding arrangement, 1 mm, 2 mm, 4 mm serially

3.3 Examination Thermal State of Model 7.3C Rate Discharge

In this regime, the research will investigate battery thermal stages at 30 m/s (108 km/h) vehicle operation speed, which is commonly referred to as highway velocity. Figure 11 describes the results of the thermal battery simulation.

Equivalent to 7.3C of battery discharge time, the amount of running current is roughly 55 A. As a result, at 60% of SOC discharged [Fig. 11d], the battery temperature exceeded the acceptable temperature of 60 °C for all of the tests. This temperature rose to 72 °C at 10% of SOC [Fig. 11a, b, c]. There is a risk of fire damage in the battery.

The reason is since the current utilized is too high, causing rapidly excessive heat production within the battery. Thus, the battery cannot efficiently cool three of the cells under the flow rate of 20 m/s ($Q = 0.02 \text{ m}^3/\text{s}$). Temperature homogeneity across the cells is not ideal, ranging from 2 °C to 4.53 °C, according to the battery differential temperature Fig. 11f. For all of these things, before switching to highway velocity, our advice is to increase the input flowrate or decrease the input air-cooling temperature by enhancing air density.

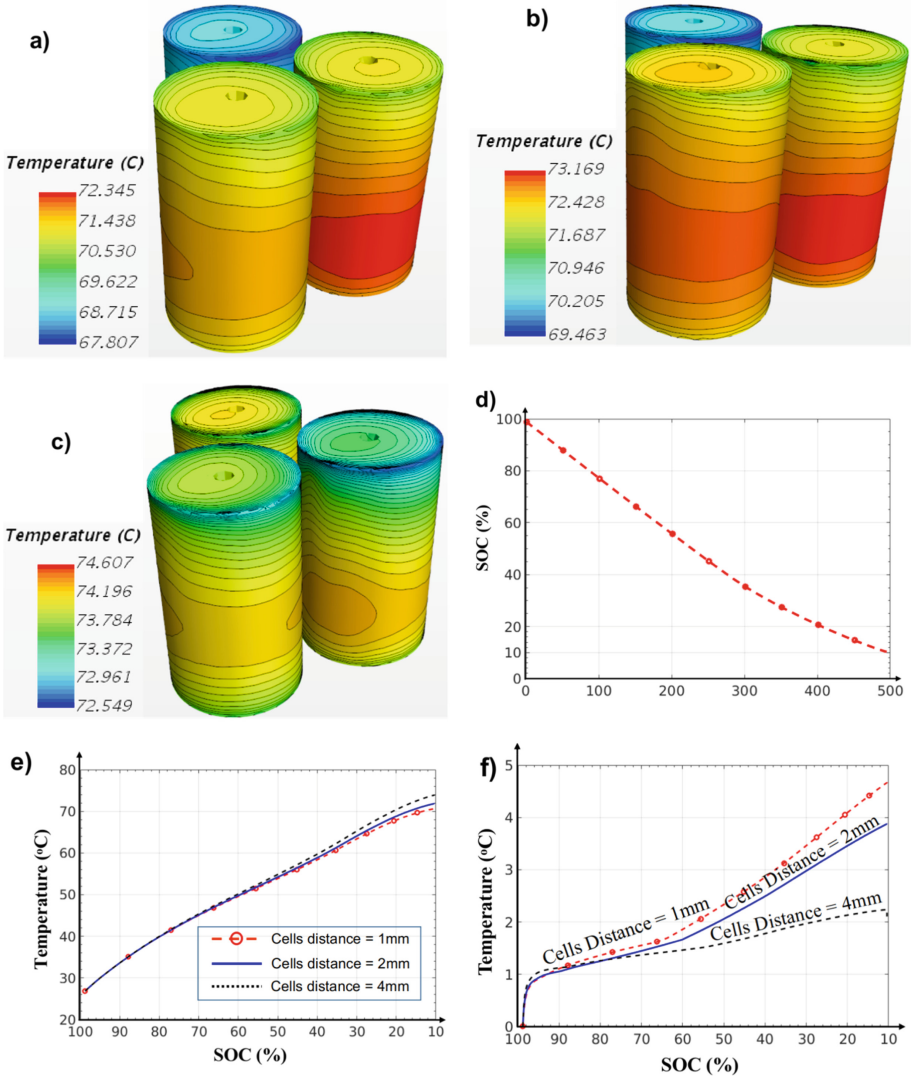


Fig. 11. The battery surface temperature at 7.3C discharge rate. (a), (b), (c) The visualization surface temperature at 10% of SOC. (d) The SOC following the 7.3C time discharge. (e) The plot of surface temperature following SOC in battery cycle life. (f) The cells differential in a case.

4 Conclusion

The forced-air cooling approach recently was found to be the most popular optimization method for battery thermal management of EVs and HEVs. By using that approach method, this work examined thermal dissipation in a model of battery mimicking a module of multiple-cell. The results showed that in the low-speed vehicle (36 km/h), the thermal of the battery is ensured. Likewise, with the same input of flowrate of 20 m/s airspeed, the surface temperature of the battery is inversely proportional to cell distance, also the cell uniformity temperature grows as cell distance increases. Conversely, the ability of air-cooling thermal management is hampered at 72 km/h due to increased heat generation; we propose keeping the battery's SOC at a higher 36% in this regime to ensure the vehicle's safety. Moreover, at highway speed (108 km/h), air-cooling systems require a larger flowrate or should reduce the temperature of the input air feed flow before entering the cooling process.

Acknowledgments. This research is funded by Hanoi University of Science and Technology (HUST) under project number T2021-PC-013.

References

1. Yang, D., et al.: The government regulation and market behaviour of the new energy automotive industry. *J. Clean. Prod.* **210**, 1281–1288 (2019)
2. Lin, B., Xu, B.: How to promote the growth of the new energy industry at different stages? *Energy Policy* **118**, 390–403 (2018)
3. Yu, H., Fan, J.-L., Wang, Y., et al.: Research on the new-generation urban energy system in China. *Energy Procedia* **152**, 698–780 (2018)
4. Zhang, Z., Wei, K.: Experimental and numerical study of a passive thermal management system using flat heat pipes for lithium-ion batteries. *Appl. Therm. Eng.* **166**, 114660 (2019)
5. Zhang, Q., Li, C., Wu, Y.: Analysis of research and development trend of the battery technology in electric vehicles with the perspective of patent. *Energy Procedia* **105**, 4274–4280 (2017)
6. RezvaniZanini, S.M., et al.: Review and recent advances in battery health monitoring and prognostics technologies for electric vehicle (EV) safety and mobility. *J. Power Sources* **256**, 110–124 (2014)
7. Rao, Z., Wang, S.: A review of power battery thermal energy management. *Renew. Sustain. Energy Rev.* **15**, 4554–4571 (2011)
8. Xu, X.M., He, R.: Research on the heat dissipation performance of battery packs based on forced air cooling. *J. Power Sources* **240**, 33–41 (2013)
9. Kizilel, R., Lateef, A., Sabbah, R., et al.: Passive control of temperature excursion and uniformity in high-energy li-ion battery packs at high current and ambient temperature. *J. Power Sources* **183**, 370–375 (2008)
10. Lyu, Y., Siddique, A.R.M., Majid, S.H., et al.: Electric vehicle battery thermal management system with thermoelectric cooling. *Energy Rep.* **5**, 822–827 (2019)
11. Wang, Q., Jiang, B., Li, B., Yan, Y.: A critical review of thermal management models and solutions of lithium-ion batteries for the development of pure electric vehicles. *Renew. Sustain. Energy Rev.* **64**, 106–128 (2016)
12. Xia, G., Cao, L., Bi, G.: A review on battery thermal management in electric vehicle application. *J. Power Sources* **367**, 90–105 (2017)

13. Kim, J., Oh, J., Lee, H.: Review on battery thermal management system for electric vehicles. *Appl. Therm. Eng.* **149**, 192–212 (2019)
14. Liu, H., Wei, Z., He, W., Zhao, J.: Thermal issues about Li-ion batteries and recent progress in battery thermal management systems: a review. *Energy Convers. Manag.* **150**, 304–330 (2017)
15. Sharma, A., Zanotti, P., Musunur, L.P.: Enabling the electric future of mobility: robotic automation for electric vehicle battery assembly. *IEEE Access* **7**, 170961–170991 (2019)
16. Gu, H.: Mathematical analysis of a Zn/NiOOH cell. *J. Electrochem. Soc.* **130**(7), 1459–1464 (1983)
17. Newman, J., Tiedemann, W.: Potential and current distribution in electrochemical cells: interpretation of the half-cell voltage measurements as a function of reference-electrode location. *J. Electrochem. Soc.* **104**(7), 1961–1968 (1993)
18. Kim, U.S., Shin, C., Kim, C.S.: Modeling for the scale-up of a lithium-ion polymer battery. *J. Power Sources* **189**, 841–846 (2009)
19. Park, C., Jaura, A.K.: Dynamic Thermal Model of Li-Ion Battery for Predictive Behavior in Hybrid and Fuel Cell Vehicles, SAE Technical Paper, 0148-7191 (2003)
20. Rao, Z., Wang, S., Zhang, G.: Simulation and experiment of thermal energy management with phase change material for aging LiFePO₄ power battery. *Energy Convers. Manag.* **52**(12), 3408–3414 (2011)
21. Park, H.: A design airflow configuration for cooling lithium-ion batteries in hybrid electric vehicles. *J. Power Sources* **239**, 30–36 (2013)
22. Yang, X.-H., Tan, S.-C., Liu, J.: Thermal management of Li-ion battery with liquid metal. *Energy Convers. Manag.* **117**, 577–585 (2016)